Organs-on-a-Chip 3 (2021) 100007

Contents lists available at ScienceDirect

Organs-on-a-Chip

journal homepage: www.journals.elsevier.com/organs-on-a-chip

Rapid 3D BioPrinting of a human iPSC-derived cardiac micro-tissue for high-throughput drug testing

Kathleen L. Miller [a], Yi Xiang [a], Claire Yu [a], Jacob Pustelnik [a], Jerry Wu [c], Xinyue Ma [a], Toshikatsu Matsui [b], Kenichi Imahashi [b], Shaochen Chen [a,c,*]

[a] Department of NanoEngineering, University of California, San Diego, 9500 Gilman Drive, La Jolla, CA, 92093, USA
[b] Takeda Pharmaceutical Company Limited, 26-1, Muraoka-Higashi 2-Chome, Fujisawa Kanagawa, 251-8555, Japan
[c] Department of Bioengineering, University of California, San Diego, 9500 Gilman Drive, La Jolla, CA, 92093, USA

ARTICLE INFO

Keywords:
3D bioprinting
Cardiac micro-tissue
Drug testing
High-throughput screening
Tissue engineering

ABSTRACT

With cardiac disease a reigning problem in the world, the need for accurate and high-throughput drug testing is paramount. 3D cardiac tissues are promising models, as they can recapitulate the cell-cell, cell-matrix, and cell-tissue interactions that impact response to a drug. Using an in-house developed micro-continuous optical printing system, we created a cardiac micro-tissue in mere seconds with microscale alignment cues in a hydrogel scaffold that is small enough to fit in a 96-well plate. The 3D printed, asymmetric, cantilever-based tissue scaffold allows one to directly measure the deformation produced by the beating micro-tissue. After 7 days, the micro-tissue exhibited a high level of sarcomere organization and a significant increase in maturity marker expression. The cardiac micro-tissues were validated against two representative drugs, isoproterenol and verapamil at various doses, showing corresponding and measurable changes in beating frequency and displacement. Such rapidly bioprinted cardiac micro-tissues in a multi-well plate offer a promising solution for high-throughput screening in drug discovery.

1. Introduction

Cardiotoxicity is a major cause of failure during drug development, a process that takes 10-15 years and costs a median of over $5 billion (Mathur et al., 2016). Moreover, cardiovascular disease is a leading health concern, accounting for 30% of deaths worldwide (Duan, 2017; Veldhuizen et al., 2019). Many drug companies employ 2D human models or mouse models to test potential drugs, but these models do not translate well to human trials. For example, 2D models do not have the complex extracellular matrix (ECM)-cell, cell-cell, and cell-tissue interactions that influence calcium handing and gene expression within cardiac tissues, leading to different responses to drugs than within humans (Mathur et al., 2016; Veldhuizen et al., 2019; Zuppinger, 2019). Moreover, mouse models, although they are able to model a complex organ response, have significant interspecies differences to humans. For instance, mice have a resting heart rate ten times higher than the average human, and a QT rate ¼ as long. Furthermore, differences in ion handling and pharmacokinetic properties prevent the mice from being a good predictive model (Veldhuizen et al., 2019; Mathur et al., 2015).

To this end, 3D engineered heart tissues have become critical as they can better recapitulate the 3D environment and its impact on the cardiac cells. To create an accurate cardiac tissue, researchers have integrated stem cell-derived human cardiac cells into models. Human induced pluripotent stem cell-derived cardiomyocytes (hiPSC-CMs) are advantageous because the stem cells can be expanded before their differentiation into cardiomyocytes. Owing to this production method, the culture of hiPSC-CMs are easier to scale up compared to that of the adult cardiomyocytes, which are difficult to procure and do not proliferate (Zuppinger, 2019). However, the maturity of hiPSC-CMs is a pervasive issue within the field (Zuppinger, 2019; Ronaldson-Bouchard et al., 2018). Newly differentiated hiPSC-CMs have many markers of immaturity, such as poor calcium handling and limited tissue alignment, which makes them poor models for a mature adult heart (Ronaldson-Bouchard et al., 2018; Guo and Pu, 2020). Various studies have investigated methods to mature the hiPSC-CMs into adult phenotypes, particularly via the alignment of the cells. Previous works have explored a variety of methods for introducing alignment, including protein-guided alignment, microgrooves, and aligned nanofibers (Mathur et al., 2016;

* Corresponding author. Department of NanoEngineering University of California San Diego 9500 Gilman Drive, Mail code 0448, La Jolla, CA, 92093-0448, USA.
E-mail address: chen168@eng.ucsd.edu (S. Chen).

https://doi.org/10.1016/j.ooc.2021.100007
Received 4 December 2020; Received in revised form 31 March 2021; Accepted 6 April 2021
Available online xxxx

Ronaldson-Bouchard et al., 2018; Agarwal et al., 2013; Ma et al., 2019). However, many of these models were 2D, and cannot fully recapitulate a 3D tissue.

To form 3D hiPSC-CM models, many researchers have simply encapsulated the cells in an ECM such as fibrin, collagen, gelatin, and/or gelatin methacrylate (GelMA) (Mathur et al., 2016; Veldhuizen et al., 2019). This allows the cells to be suspended in a 3D space as they spread and form connections. However, many of these 3D models did not use direct alignment cues for the cardiac cells. In substitute, some models incorporate two pillars on either side of the tissue that move when the tissue contracts. This constant stress on the tissue enhances cardiac alignment, with the added benefit of accurately measuring the contractility of the tissue. A common method for producing these models is to first produce molded PDMS pillars. These are then cultured upside-down in a pool of cell and ECM suspension. Over time, the cells naturally adhere to and organize around the pillars, displacing them as they begin to exhibit a beating phenotype (Mathur et al., 2016; Ronaldson-Bouchard et al., 2018; Ma et al., 2018, 2019; Hinson et al., 2015; Hansen et al., 2010; Boudou et al., 2012; Nunes et al., 2013; Tiburcy et al., 2020; Liu et al., 2020). The models have a large range in size, from about a length of 500 μm to a length of 5 mm, as well as a variety of tracking methods, from grayscale tracking to embedded fluorescent beads. The relatively simple fabrication of these models has also translated into established protocols and commercial products, such as those produced by Tiburcy et al. and the Biowire™, respectively (Nunes et al., 2013; Tiburcy et al., 2020). Nevertheless, these tissues rely on the tension force of contracting cells to align the cardiomyocytes. Research suggests that by incorporating 3D alignment cues in the matrix, a more organized tissue can be formed (Liu et al., 2020).

Creating 3D alignment cues in tissues can be best addressed by 3D bioprinting. By mixing cells in ECM, a 3D printer can specify the initial location of the cardiac cells with the ECM, acting as 3D physical and biochemical guidance during culture. Our recently developed micro-continuous optical printing system (μCOP) is an ideal 3D bioprinting method for its superior printing resolution, speed, and biocompatibility (Ma et al., 2016, 2019; Liu et al., 2020; Yu et al., 2020). The μCOP system uses a UV-light to polymerize a pre-polymer solution per optical patterns, thereby creating a 3D hydrogel construct encapsulating biological cells. Due to the printer's rapid printing nature, cells spend minimal time outside of culture, making the system advantageous to slower, extrusion-based printers. Many photopolymerizable ECMs have been developed for use in both acellular and cellular printing, such as GelMA, poly(ethylene glycol) diacrylate (PEGDA), glycidyl methacrylate-hyaluronic acid (HAGM), and thiol-ene gelatin (Ma et al., 2016; Bertlein et al., 2017; Lim et al., 2018; Lin et al., 2013). GelMA is a popular photopolymerizable ECM for bioprinting encapsulated cells due to the natural degradation and adhesion moieties presented by gelatin, making it easily reorganized by cells (Munoz et al., 2014). The methacrylate groups functionalized onto the gelatin backbone undergo free-radical polymerization, quickly propagating in selected areas exposed to UV-light. By adjusting both the light exposure time and the concentration of GelMA, the hydrogel pore size changes, thereby impacting hydrogel stiffness, which can be tuned according to the tissue system (Yu et al., 2020). The free radicals are generated via a photo-initiator, which produces radicals upon exposure to certain wavelength of light. Within our bioprinting, a low intensity, 365 nm UV light is used to induced free-radical generation. Compared to middle-UV light (e.g. 254 nm), 365 nm UV light has been shown to have a limited impact on proliferation and protein expression, even after exposure for 10 min (Ruskowitz and Deforest, 2019; Fairbanks et al., 2009). Thus with short exposure time (<60s) and low intensity, the damage that the 365 nm UV caused on the cells during fabrication with our μCOP system is minimal.

Using the μCOP system, we printed a cardiac micro-tissue with 3D alignment. The micro-tissue fits onto a 5 mm coverslip, which is then transferred to the well of a 96-well plate for rapid drug testing. This process is novel as many comparable miniature models do not have initial 3D-alignment, but develop it purely from stress cues (Mathur et al., 2015; Ma et al., 2019; Boudou et al., 2012; Huebsch et al., 2016). Moreover, we successfully differentiated, cultured, and printed hiPSC-CMs into the scaffold and demonstrated their increase in maturity over 7 days. Significantly, we incorporated fluorescent beads to the pillar set-up to enable more robust tracking of the tissue contraction in smaller dimensions. By tracking the small pillar, we evaluated the micro-tissue response to both isoproterenol (ISO) and verapamil (VERA). This miniaturized tissue chip is a promising tool for both drug discovery and screening.

2. Materials and methods

2.1. Methacrylated coverslip preparation

Glass coverslips were functionalized with methacrylate groups to allow the printed hydrogels to stick to the coverslip; during photopolymerization, the methacrylate groups on the coverslips react with the acrylate groups in the hydrogel. To functionalize, first a 1:10 mixture of acetic acid (Cat. # 320099-500 ML, Sigma-Aldrich) to 100% ethanol (Cat#. 459836-1L, Sigma Aldrich) was produced. Next, a solution 1.75%(v/v) 3-(Trimethoxysilyl)-Propyl Methacrylate (TMSPMA) (Cat. #, M6514-50 ML, Sigma-Aldrich), 10.5%(v/v) 1:10 acetic acid: ethanol, and 87.75%(v/v) 100% ethanol was added to a 50 mL conical. 5 mm round coverslips were then added to the conical, with the solution approximately double the volume of coverslips, and left on the rocker overnight for incubation at room temperature. The next day, the coverslips were washed twice with 100% ethanol, twice with MilliQ water, and left to dry at room temperature. Methacrylated coverslips were stored under aluminum foil and left at room temperature.

2.2. GelMA synthesis

Methacrylated gelatin (GelMA) was synthesized according to previously published protocols (Nichol et al., 2010; Gauvin et al., 2012). Briefly, gelatin (Cat. #G2500, Sigma-Aldrich) was dissolved in 60°C 1x PBS (Cat. #14190144, Gibco) at 1%(w/v) and stirred until dissolved. Methacrylic anhydride (Cat. # 276685, Sigma Aldrich) was then added dropwise to 8%(v/v) and reacted for 3 h. The reaction was quenched by a 2x dilution with additional 60°C 1x PBS and allowed to stir for another 15 min. The solution was then dialyzed against 40°C MilliQ water for one week using 12-14 kDa cutoff dialysis tubing (Cat. #132706, Spectrum Labs). After dialysis, the solution was lyophilized for three days and stored at −80 °C until further use.

2.3. HAGM synthesis

Hyaluronic acid glycidyl methacrylate (HAGM) was synthesized according to previously published protocols (Suri et al., 2011). Briefly, 1% (w/v) of sodium hyaluronate (Cat. #HA5K-5, Lifecore Biomedical) was dissolved in a 1:1 solution of water: acetone at room temperature overnight. A 20-fold molar excess (7.2%(w/v)) of triethylamine (Cat. # 471283, Sigma-Aldrich) was then added dropwise to the solution and reacted for 30 min. Directly following, a 20-fold molar excess (7.2%(w/v)) of glycidyl methacrylate (Cat. #151238, Sigma Aldrich) was added dropwise, and the solution reacted overnight. The solution was then washed with 4 L of acetone via filtration. The resulting precipitate was dissolved in MilliQ water and dialyzed against MilliQ water for 12 h using 3.5 kDa cutoff dialysis tubing (Cat. #132592, Spectrum Labs). After dialysis, the solution was lyophilized for three days and stored at −80 °C until further use.

2.4. LAP synthesis

Lithium phenyl-2,4,6-trimethylbenzoylphosphinate (LAP) was synthesized according to previously published protocols (Fairbanks et al.,

2009). Briefly, 3.2 g of 2,4,6-trimethylbenzoyl chloride (Cat. #C965Y83, Thomas Scientific) was added dropwise to 3 g of dimethyl phenylphosphonite (Cat. #149470, Sigma-Aldrich) and reacted under argon gas for 18 h. After heating the mixture in a water bath to 50 °C, 6.1 g lithium bromide (Cat. #213225, Sigma-Aldrich) dissolved in 100 mL of 2-butanone (Cat. #M209-4, Thermo Fisher Scientific) was added dropwise and reacted for 10 min. The reaction was cooled at room temperature for 4 h, after which the resulting precipitate was washed with 400 mL of 2-butanone (Cat. #M209-4, Thermo Fisher Scientific) via filtration. The washed precipitate was dried overnight, then collected and stored at room temperature under argon until use.

2.5. Prepolymer solution preparation

Stock solutions were prepared as follows; lyophilized GelMA and HAGM foams were dissolved in 1x PBS at 37 °C at 20%(w/v) and 8%(w/v) stock solutions, respectively, sterilized with a 0.22 μm filter (Cat. #SCGP00525, Millipore Sigma), and stored at 4 °C. Powdered LAP was dissolved in 1x PBS at 37 °C to 4%(w/v), sterilized with a 0.22 μm filter, and stored at 4 °C.

To prepare prepolymer solutions, stock solutions were first warmed to 37 °C. The stock solutions were then added to the appropriate concentration for each prepolymer solution, as outlined in Table S1, vortexed, and then stored in 4 °C until printing. The prepolymer solution for the base layer was 2% HAGM, 2% PEGDA700 (Cat. #455008-500 ML, Sigma Aldrich), and 1% LAP. The pillar layer was printed using 15% GelMA, 0.2% LAP, and 1% AF555 fluorescent beads (Cat. #F13082, Thermo Fisher Scientific). The cell-encapsulated line layer was fabricated using 7.5% GelMA and 0.6% LAP, and the cells were added directly before printing.

2.6. Human iPSC culture and cardiac differentiation

Human iPSCs were re-programmed as previously described and maintained in Essential 8 medium (Cat. #A1517001, ThermoFisher Scientific) (Ma et al., 2019). For maintaining culture, 6-well plates were coated with hESC-qualified Matrigel (Cat. #354277, Corning) and split 1:6 every 3-4 days with Versene (Cat. #15040066, ThermoFisher Scientific). For differentiation, 12-well plates were coated with Matrigel and seeded at 1:6 and culture until reaching 80% confluency. Differentiation was initiated using the PSC Cardiomyocytes Differentiation kit (Cat. #A2921201, ThermoFisher Scientific). Briefly, cells were first cultured with differentiation media A for 2 days, differentiation media B for another 2 days, and then differentiation maintenance media for 8 days. Following the completion of the differentiation, cells were purified with RPMI medium without glucose (Cat. #11879020, ThermoFisher Scientific) supplemented with 4 mM lactate (Cat. #129-02666, Wako Chemicals) for 6 days. The purified cells were then cultured in HEPES buffered RPMI1640 medium (Cat. #22400089, ThermoFisher Scientific) supplemented with 2%(v/v) B27 (Cat. #17504044, ThermoFisher Scientific) until printing. To prepare for mixing into the prepolymer solution, the cells were first incubated at 37 °C with 0.5%(w/v) collagenase (Cat. #07427, STEMCELL Technologies) dissolved in DMEM/F-12 media (Cat. # 11320033, ThermoFisher Scientific) for 15 min to digest extracellular matrix. The cells were lifted by incubating with 0.25% trypsin-EDTA for 5-7 min, centrifuging at 200 g for 3 min, and resuspending in RPMI1640 medium with 20%(v/v) FBS (Cat. #16140071, ThermoFisher Scientific) and 5 μM ROCK inhibitor Y-27632 (Cat. #72304, STEMCELL Technologies). The cells were aliquoted in microcentrifuge tubes, spun down once more at 200 g for 3 min, and kept on ice until resuspension with lifted Normal Human Ventricular Cardiac Fibroblasts (HCFs) at a ratio of 10:1 in the prepolymer solution, with a final concentration of 50 million cells/mL (45 million iPSC-CMs/mL:5 million HCFs/mL).

2.7. Human cardiac fibroblast culture

HCFs (Cat. # CC-2904, Lonza) were cultured in flasks with FGM-3 media (Cat. # CC-4526, Lonza). Briefly, cells were cultured until 70% confluency, at which point they were subcultured at a 1:4 ratio. HCFs were brought to confluency before use for printing and used between passages 5 and 9.

2.8. 3D printing of micro-tissue construct

To build the construct, we used the in-house μCOP printer. Briefly, the printer consists of the followings: (i) a 365 nm UV LED light source; (ii) a digital micromirror array device (DMD) composed of approximately 2 million micromirrors for light projection; (iii) projection optics that focus the optical patterns from the DMD chip onto the fabrication plane; (iv) a motorized x-y-z stage; and (v) a computer control unit. The pattern for each layer was designed in Adobe Photoshop and converted to PNG images compatible with the printer software. For each layer, polydimethylsiloxane (PDMS) spacers were used to control the Z-thickness and placed upon a 5 mm methacrylated coverslip. A PDMS coated coverslip was used to top the set-up, and the relevant prepolymer solution heated to 37 °C was pipetted between the spacers. The set-up was then placed on the motorized stage, and the prepolymer solution was then polymerized by projected light pattern. Between each layer, warmed 1x PBS was used to wash away the extra prepolymer solution. After printing the first two layers (the base and pillar layers), the cells were added to the GelMA prepolymer solution to print the lines scaffold encapsulating the cells. The supernatant of the cell pellet consisting of cardiomyocytes and human cardiac fibroblasts was diluted to 50 million cells/mL by gently mixing with the GelMA prepolymer solution. This mixture was directly added to the set-up in order to reduce the amount of time the cells spent in the prepolymer solution. The printing time for this cell printing step is only 17.5 s. See Supplementary Fig. S1 for a schematic and Supplementary Fig. S2 for the printing parameters.

2.9. Immunofluorescent staining and imaging

Differentiated hiPSC-CM samples were stained with Human Cardiomyocyte Immunocytochemistry Kit (Cat. # A25973, ThermoFisher Scientific) to confirm NKX2.5 and TNNT2 presence. Briefly, samples were incubated with 4%(w/v) paraformaldehyde (PFA) (Cat. # A24344, ThermoFisher Scientific) solution. Next, samples were permeabilized for 15 min with 1% Saponin (Cat. # A24878, ThermoFisher Scientific) and then blocked with 3% bovine serum albumin (BSA) (Cat. # A24353, ThermoFisher Scientific) for 30 min. Samples were then incubated overnight at 4 °C with primary antibodies, anti-NKX2.5 (Cat. # A25974, ThermoFisher Scientific) and anti-TNNT2 (Cat. # A25969, ThermoFisher Scientific), diluted at 1:1000 in 3% BSA solution. The next day, samples were incubated for 1 h at room temperature with Alexa Fluor® 555 donkey anti-rabbit (Cat. # A25971, ThermoFisher Scientific) and Alexa Fluor® 488 donkey anti-mouse (Cat. # A25972, ThermoFisher Scientific), diluted at 1:250 in 3% BSA solution. Lastly, the cells were incubated with NucBlue® Fixed Cell Stain (DAPI) (Cat. #R37606, ThermoFisher Scientific) for 5 min before storing in 1x PBS at 4 °C and imaged within 1 month.

Full cardiac micro-tissues were stained for actinin. Samples were fixed in 4%(w/v) PFA (Cat. #J61899-AP, Alfa Aesar) solutions for 15 min on day 7 following printing. Samples were then blocked and permeabilized with 2%(w/v) BSA solution (Cat. #X100-500 ML, Sigma Aldrich) with 0.1%(v/v) Triton X-100 (Cat. #A8806-5G, Sigma Aldrich) for 1 h at room temperature. Subsequently, samples were incubated overnight at 4 °C with Anti-Sarcomeric Alpha Actinin antibody (Cat. #9465, Abcam) diluted at 1:100 in 2% BSA. Samples were then incubated with Phalloidin-iFluor 647 Reagent (Cat. #ab176759, Abcam). Lastly, the cells were incubated with NucBlue® Fixed Cell Stain (DAPI) for 15 min before storing in 1x PBS at 4 °C and imaged within 1 month.

2.10. RNA isolation and Reverse Transcription-Polymerase Chain Reaction (RT-PCR)

RNA extraction was performed using Direct-zol™ RNA MicroPrep Kit (Cat#. R2061, Zymo Research). Briefly, samples were incubated with TRI Reagent® and stored in a −80 °C freezer. Later, samples were thawed to room temperature and processed with the MicroPrep Kit to collect the RNA from the samples. RNA was then converted to cDNA using the ProtoScript® First Strand cDNA Synthesis Kit (Cat#. E6300S, New England BioLabs), following the manufacturer's instruction on a QuantStudio 3 PCR System. cDNA was stored at −20 °C until ready for real-time PCR (RT-PCR). For RT-PCR, the Luna® Universal qPCR Master Mix (Cat. #M3003S, New England BioLabs) was used according to the manufacturer's instruction with the QuantStudio 3 PCR System. The forward and reverse primers, purchased from Integrated DNA Technologies and detailed in Supplementary Table S3, were diluted in UltraPure™ DNase/RNase-Free Distilled Water (Cat. # 10977015, ThermoFisher Scientific). The relative quantification was calculated based on the threshold cycle (Ct) and normalized against the housekeeping gene, glyceraldehyde 3-phosphate dehydrogenase (GAPDH).

2.11. Drug incubation

Two drugs were used to evaluate the hiPSC-CM construct: isoproterenol (ISO) (Cat. #420355-100 MG, Millipore Sigma) and verapamil (VERA) (Cat. #PHR1131-1G, Sigma Aldrich). Stock solutions for each drug were prepared with Dimethyl sulfoxide (DMSO) (Cat. #D12345, ThermoFisher Scientific) or UltraPure™ DNase/RNase-Free Distilled Water (Cat. # 10977015, ThermoFisher Scientific) and stored in −20 °C. On the day of testing, samples were thawed to room temperature and diluted in Tyrode's solution to the various drug doses (see Supplementary Table S4 for further details). To test the various drugs, constructs were incubated in Tyrode's solution at 37 °C for 15 min. Samples were then paced at 0 Hz, 0.5 Hz, 0.8 Hz, 1 Hz, 1.5 Hz, and 2 Hz and each frequency was recorded for 250 frames on a fluorescent microscope. For each subsequent drug dose, 10% of the Tyrode's volume was removed, replaced with the appropriate drug dose, and left to equilibrate for 15 min before recording the various pacing frequencies.

2.12. Displacement measurement

The displacement of the small pillar was measured under a Leica DMI 6000B fluorescent microscope using a 10X objective lens focused as the top of the pillar. A customized MATLAB script was developed in-house to track the average weighted mean of bead fluorescence, from which displacement and BPM were calculated.

2.13. Image acquisition and processing

Confocal microscope images were acquired with a 20X water-immersion objective attached to a Leica SP5 confocal microscope. ImageJ (National Institutes of Health) was used to merge channels, generate z-projection and carry out measurements for images and stacks.

2.14. Quantification of sarcomere length and orientation

The sarcomere length and orientation were measured based off the confocal images of tissue stained with alpha-actinin. The sarcomere length was measured by using the line tool and finding the average band length among approximately 100 sarcomeres. The orientation of the sarcomeres was analyzed using the directionality tool in ImageJ.

2.15. Statistical analysis

All data are expressed as a mean ± standard deviation (SD). Statistical analyses were performed with GraphPad Prism version 6.0 Software by one-way ANOVA with Tukey's post-hoc comparison. Significant differences were considered when $p<0.05$.

3. Results and discussion

3.1. 3D printing of hiPSC-CM scaffold

In this study, we printed 3D micro-tissues comprised of hiPSC-CMs and HCFs for drug testing. Human iPSCs were differentiated over 18 days (Supplementary Fig. S1), during which time they deposited a lot of ECM. As seen in Supplementary Fig. S2, the differentiated cells formed tissues of varying concentrations across the well, in more "2D"-like areas and "3D"-like areas. Generally, the "3D"-like areas appeared to have a higher expression of TNNT2 and NKX2.5, possibly due to either a more mature phenotype or higher concentration of cells. However, the excess amount of ECM produced during differentiation led to difficulties in printing processing and final cell concentration, so we incubated the cells with collagenase for 15 min before lifting off the cells. Although this step removed some of the cells from the "2D"-like areas, it kept the cells from the "3D"-likes areas and aided immensely in processing (Supplementary Fig. S2).

Using the μCOP system, we formed a scaffold from three steps on a 5 mm round coverslip (Fig. 1A and B, Supplementary Fig. S3). In Step 1, a base layer comprised of HAGM and PEG700 was printed to prevent extraneous cell growth from proliferating HCFs. After washing away the material with PBS, we proceeded to Step 2, where a pillar layer comprised of GelMA and encapsulated with fluorescent beads of 1 μm in diameter was printed. The pillars were designed to be two vastly different sizes; in this way, only the small pillar will deform significantly upon tissue contraction, which in turn makes calculating the force of contraction much easier. We also monitored the pillars over 7 days, finding that their dimensions unchanged (Fig. 1C). Lastly, for Step 3, a cell mixture of hiPSC-CMs and HCFs (10:1) was encapsulated in GelMA to a final concentration of 50 million cells/mL in a lines pattern. The lines were 30 μm thick with 50 μm spacing. Fig. 1D shows example acellular images of each step from both aerial and side views for clarity.

3.2. Examining the hiPSC-CM micro-tissue at 7 days

After printing the scaffolds, the tissues were cultured in media for 7 days, with media changes every 2 days. Over the 7 days, due to the adhesion and degradation moieties innate in gelatin, the HCF and hiPSC-CMs were able to reform and form a compact tissue (Fig. 2A). After 3 days, most of the hiPSC-CMs regained their beating phenotype and began to beat as a full tissue by Day 7 as the number of intercellular connections increased (Supplementary Video 1).

The beating tissue caused contraction of the small pillar, which we used to track displacement and beats per minute (BPM). To create a robust tracking method, we encapsulated fluorescent beads into the small pillar during printing. This allows us to see the displacement of the small pillar, even if overgrowth of cells on the pillar, or another visual issue, prevented reliable grayscale tracking in the brightfield channel. To track the pillar, we took a video in the fluorescent channel and then cropped our image around a clear fluorescent bead. By using an in-house designed MATLAB script, the displacement of the bead was tracked over time, producing a time vs displacement graph (Fig. 2B). From this graph, important parameters such as average BPM and average displacement were calculated.

We also found that by 7 days the micro-tissue displayed a high level of organization. After staining for sarcomere alignment, the mean degree value was 89.6° with a standard deviation of 21.8°. Compared to a similar method using seeded cells, our encapsulated cells within lines showed a higher level of alignment of the hiPSC-CMs (Ma et al., 2019). These results indicate a better replicate of a mature phenotype and can improve the contraction force, as the hiPSC-CMs are contracting in the

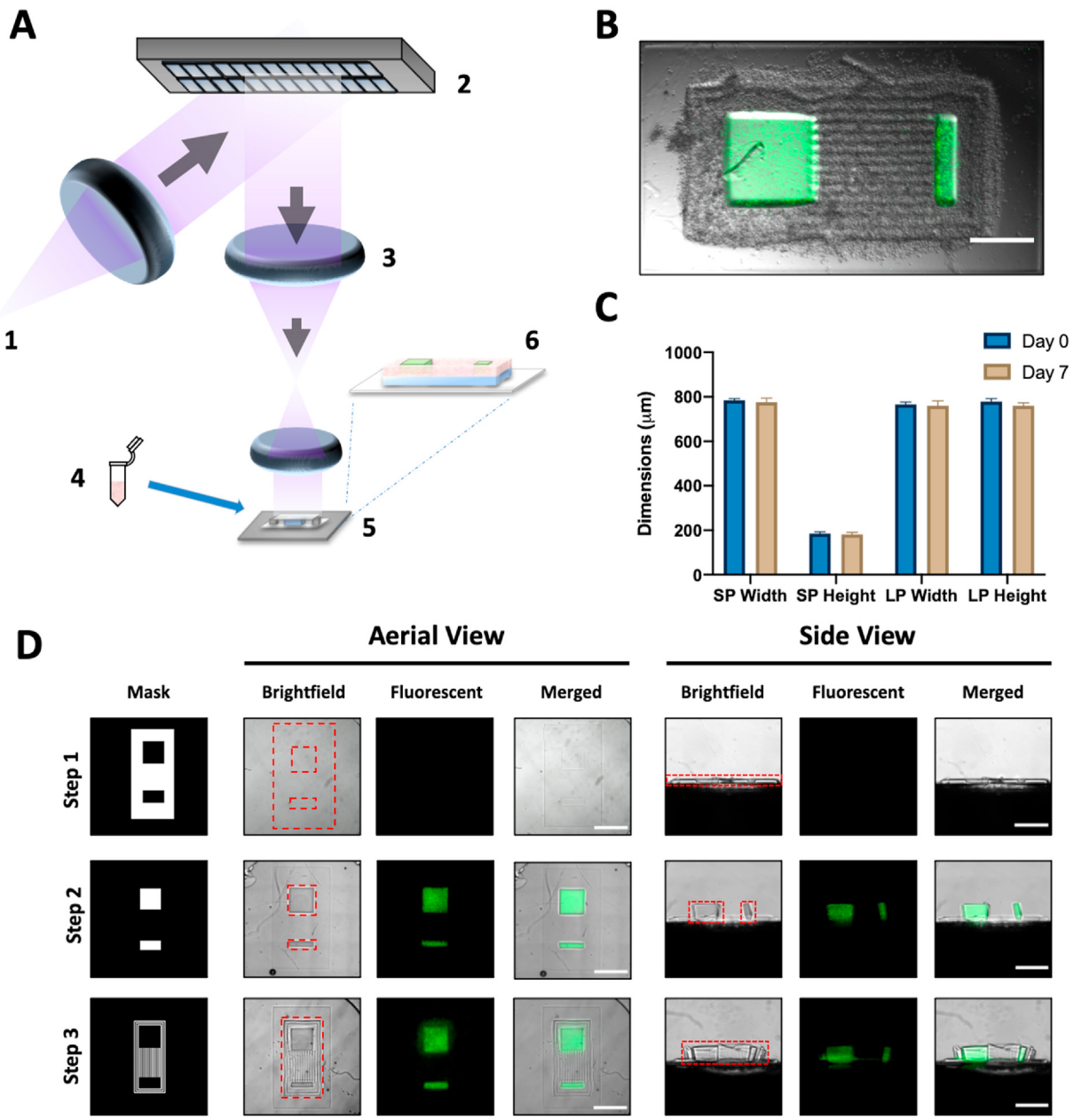

Fig. 1. Fabrication of the cardiac micro-tissue. (A) Schematic of DLP-based bioprinter consisting of a (1) UV light source, (2) DMD, (3) focusing optics, (4) prepolymer solution, and (5) 3D sample stage for fully printed scaffold. (B) Merged fluorescent and brightfield image of fully printed representative sample with encapsulated cells (scale bar = 500 μm). (C) Graphs displaying dimensions of both the small pillar (SP) and large pillar (LP) in the scaffold over 7 days (N = 8). (D) Example images showing printing steps in 3D scaffold (scale bar = 1000 μm).

same direction. However, the average sarcomere length was 1.86 μm with a standard deviation of 0.29 μm. This is similar to results found by other groups using hiPSC-CMs, but less than the adult sarcomere length of 2.2 μm that some models exhibit (Ronaldson-Bouchard et al., 2018; Guo and Pu, 2020; Ma et al., 2019; Mannhardt et al., 2016).

3.3. Evaluating the maturity of micro-tissues via qPCR

One important challenge of a hiPSC-CMs-based tissue model is its relative immaturity compared to the adult heart. This difference can impact the tissue's relative response to a drug, making the results less translatable to human trials (Ronaldson-Bouchard et al., 2018). To examine the maturity of the cells in the 3D printed tissue, we evaluated the relative RNA expression of 8 different maturity markers (Fig. 3). After 20 days of differentiation, the hiPSC-CMs were cultured for up to 46 total days. During this time, cells were taken at various points for either 2D culture RNA samples (after being mixed with a 1:10 ratio of HCF:hiPSC-CM) or encapsulated within the 3D micro-tissue, cultured for 7 days, and then taken for RNA samples. qPCR was then performed on the samples, evaluating the expression of various genes relative to GAPDH in each sample. The calcium handling of the 3D tissue was analyzed by the CACNA1C (subunit of voltage dependent calcium channel), RYR2 (ryanodine receptor), and SERCA2a (sarcoplasmic/endoplasmic reticulum calcium ATPase) expression levels. Both CACNA1C and RYR2 were significantly higher than the corresponding 2D cultured cells. Although not statistically significant, SERCA2a displayed an upward trend in expression level similar to other 3D heart tissues (Mannhardt et al., 2016; Kranias and Hajjar, 2012; Rao et al., 2013; Turnbull et al., 2014) (Fig. 3Bi-iii, Supplementary Figure S4i-iii). The increase in expression of CXN43 (gap junction protein) appears to indicate that cells were able to

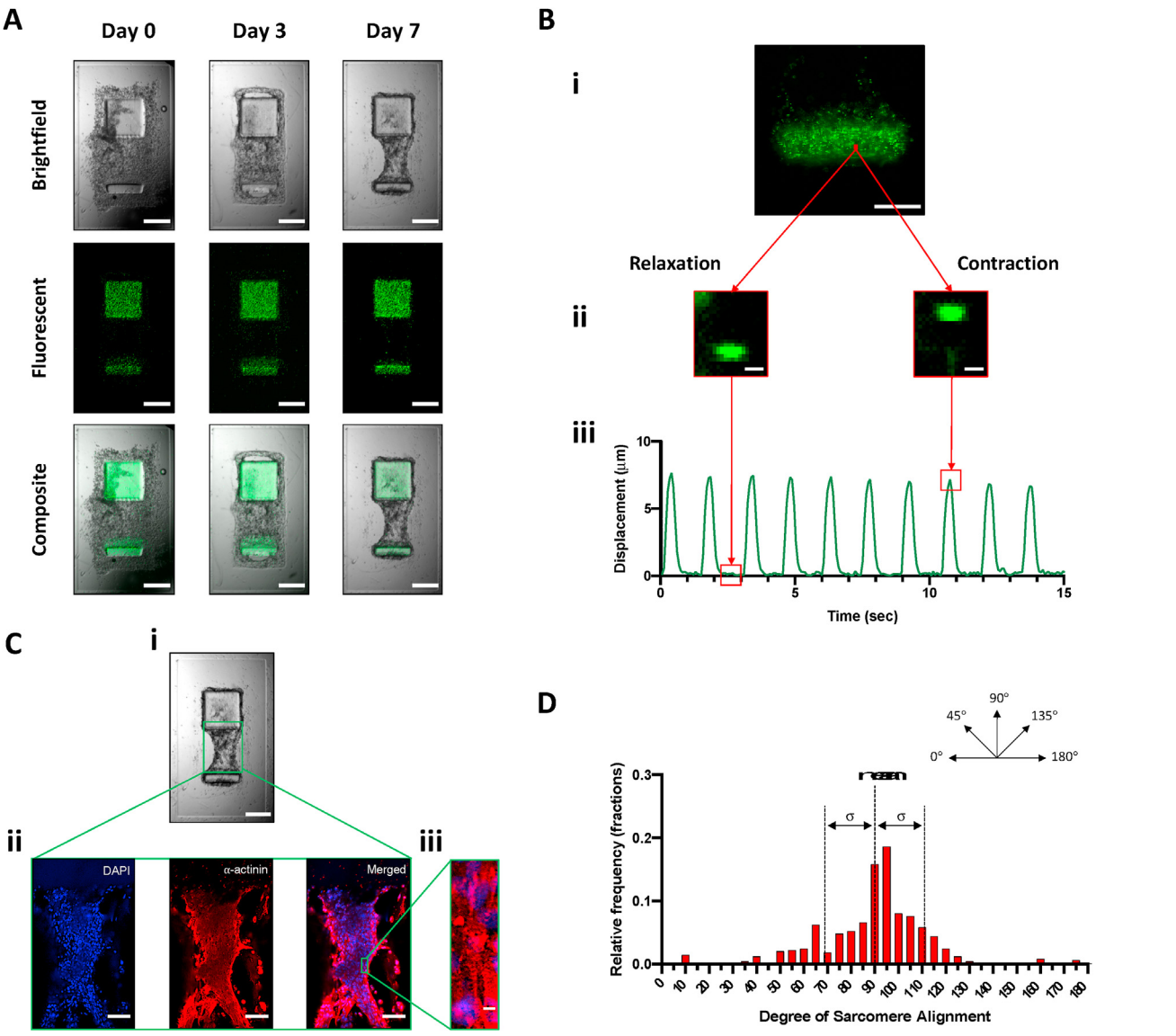

Fig. 2. (A) Images showing cardiac micro-tissue over 7 days (scale bar = 250 μm). (B) Fluorescent beads are used for tracking displacement of the small pillar and calculating BPM of the cardiac micro-tissue. (i) An example fluorescent image of the small pillar is cropped to focus on one bead. (ii) The corresponding relaxation and contraction points of the tissue in the cropped image. (iii) The resulting graph showing beating phenotype of the tissue. (C) (i) An example day 7 scaffold (scale bar = 250 μm) stained for (ii) DAPI and α-actinin to analyze sarcomere alignment (scale bar = 250 μm). (iii) A zoom image of the merged image displaying sarcomere alignment (scale bar = 5 μm. (D) A histogram showing the alignment of sarcomeres measured from confocal images of micro-tissues at day 7 (N = 5 samples, mean = 89.6°, σ = 21.8°).

exchange ions more efficiently, better mimicking a mature heart tissue (Sottas et al., 2018) (Fig. 3Biv). However, when extending this comparison to pure population controls of HCF and hiPSC-CM, there is no significant difference between the mixed population cell control and the day 7 micro-tissue (Supplementary Fig. S4iv). This suggests that the increase in CXN43 included a contribution from HCF cell population increase over 7 days, as HCF will proliferate whereas the hiPSC-CM will not. A population of analysis of the day 7 micro-tissues would be necessary to fully decipher these results. In addition to calcium handling, the expression of genes related to sarcomeres was analyzed; MYH6 (α myosin heavy chain), MYH7 (β myosin heavy chain), MLC2C (myosin light chain), and TNNT (cardiac muscle troponin T) (Fig. 3Bv-viii, Supplementary Fig. S4v-viii). These four genes contribute to the formation of sarcomeres, which are formed during human iPSC differentiation (Seguchi et al., 2007; Salick et al., 2014). As the cells gain a more mature phenotype, the myofibrils are expanded with additional sarcomeres, and thus these four genes are more heavily expressed.

3.4. Testing the drug response of micro-tissues

The most important aspect of the micro-tissues is their ability to respond to drugs in measurable parameters. The more mature the micro-tissue, the more mature their calcium handling, which in turn impacts the contractility force and drug response of the iPSC-CMs. To evaluate the functionality of the micro-tissues, we incubated the samples with progressively higher doses of two common cardiac related drugs, isoproterenol (ISO) and verapamil (VERA). ISO is a non-selective beta-adrenergic agonist. As the beta-adrenergic receptor system relies on effective calcium handling, it is a common drug used to test for maturity (Ronaldson-Bouchard et al., 2018). Within literature, cardiac cells are often dosed within the range of 0.01 nM to 1 mM, with 100 nM the most common dose. The efficacy of isoproterenol is then commonly measured via calcium transients (Ronaldson-Bouchard et al., 2018; Rao et al., 2013), as the response is most significant in this analysis, but it can also be measured via twitch force (analogous in our set-up to displacement),

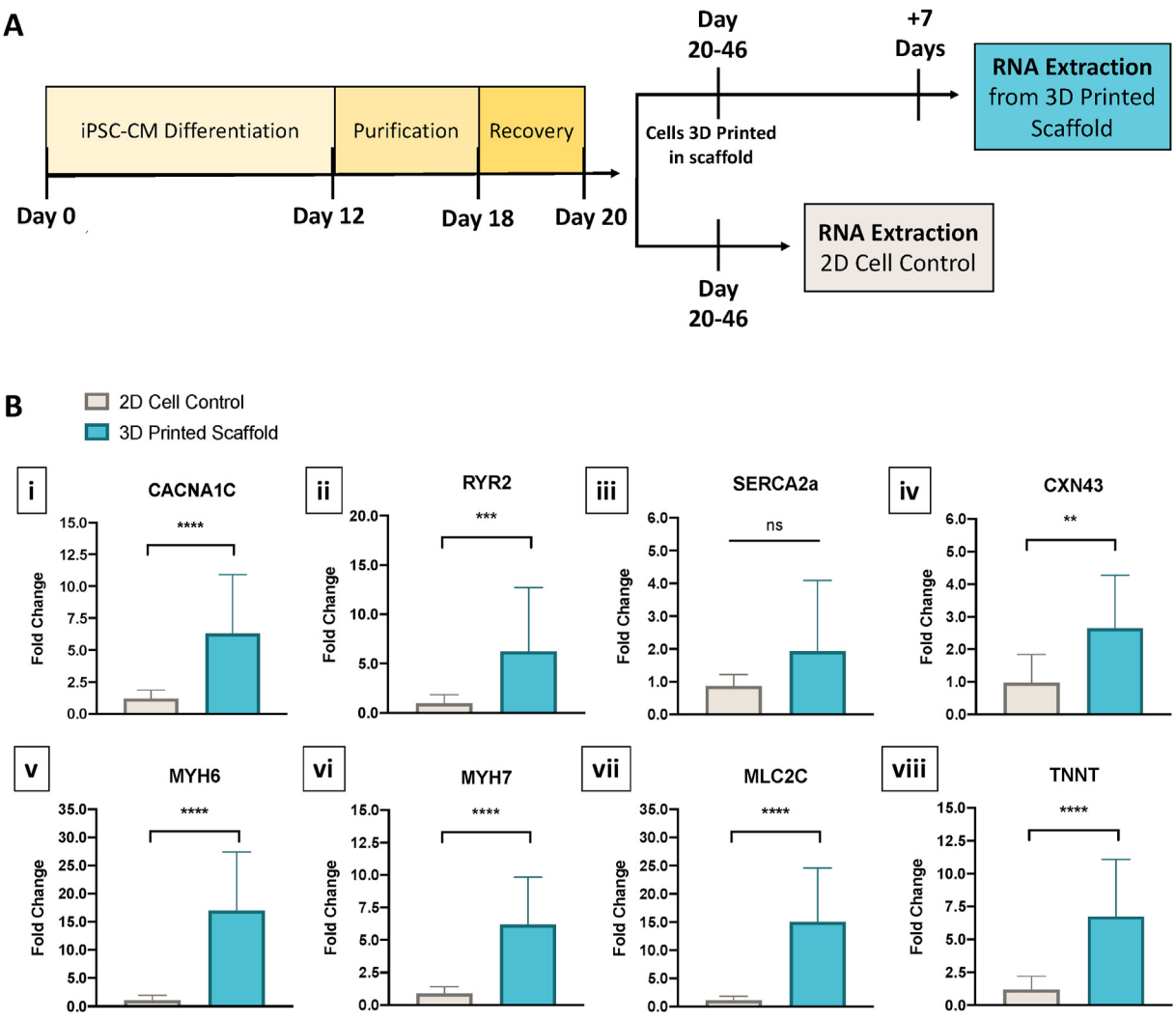

Fig. 3. 3D printed cells in micro-tissue mature more than 2D cultured cells. (A) Schematic outlining cell cultivation before RNA extraction. (B) Plots showing gene expression fold change of iPSC-CM cultured under two different approaches for CACNA1C, RYR2, CXN43, MLC2C, MYH6, MYH7, and TNNT. Mean ± SD, N = 6-24, **p ≤ 0.005, ***p ≤ 0.0005, ****p ≤ 0.0001, unpaired *t*-test.

BPM, width at half peak height (W_{50}), and relaxation time (Ma et al., 2019; Huebsch et al., 2016) (Supplementary Fig. S5A). Seeing a response in these parameters is valuable as it eradicates a Ca^{2+} staining step and simplifies analysis. To evaluate our micro-tissues, we dosed our samples with ISO at 0.1 nM, 1 nM, 10 nM, and 100 nM. In addition, we also recorded the micro-tissue response to being paced at 0.5 Hz, 0.8 Hz, 1.0 Hz, 1.5 Hz, and 2 Hz at each dose. Similar to other reports of hiPSC-CM based tissues, we observed an increase in displacement for unpaced tissues at 100 nM (N = 4), as well as an increase in BPM starting at 0.1 nM (N = 4) (Fig. 4A and B) (Ronaldson-Bouchard et al., 2018; Ma et al., 2018; Huebsch et al., 2016). Notably, samples were also able to robustly catch higher frequencies (2 Hz) during electrical pacing after 1 nM (Supplementary Fig. S4Bii). Moreover, the W_{50} and relaxation time (at 80% peak height and 90% peak height, denoted RT_{80} and RT_{90}, respectively) showed significant changes at even lower doses. A significant decrease in W_{50} was observed at both 100 nM and 10 nM ISO (N = 4), similar to results seen by Takeda et al. (2018). In addition, both RT_{80} and RT_{90} were calculated in order to compare to other results in literature, as calculated relaxation peak height varies among groups. We found a significant decrease in both RT_{90} and RT_{80} at 1 nM, 10 nM, and 100 nM (N = 4) (Fig. 4D, Supplementary Fig. S4Bvi), which is comparable to results found by other groups (Mannhardt et al., 2016; Stoehr et al., 2014). However, the paced-trained cardiac tissues produced by Ronaldson-Bouchard et al. found a decrease in RT_{90} as low as 0.01 nM ISO, suggesting that further sensitivity in our micro-tissues can be achieved (Ronaldson-Bouchard et al., 2018). The micro-tissues were also evaluated by dosing with 1 nM, 10 nM, and 100 nM VERA in a 1.2 mM Ca^{2+} Tyrode's solution at 0 Hz, 0.5 Hz, 0.8 Hz, 1.0 Hz, 1.5 Hz, and 2 Hz. VERA acts in a two-fold fashion, binding to (and thereby interfering with) two different channels, the *L*-type calcium channels and hERG channels, which have opposing actions on the action potential duration (Sanguinetti and Tristani-Firouzi, 2006; Lind et al., 2017). We observed no change in BPM for the unpaced tissues, which is consistent with other studies for similar 3D heart tissues (Mathur et al., 2015; Huebsch et al., 2016). However, there was a downward trend in the ability for the micro-tissues to catch higher frequencies in higher doses (Supplementary Fig. S4Cii). Over the same dose range for unpaced micro-tissues, we also observed a trend in declining displacement values (N = 4) (Fig. 4D), which is consistent with previous results (Mannhardt et al., 2016; Turnbull et al., 2014; Okai et al., 2020). This trend was significant at 100 nM VERA, and was also consistent at all paced frequencies (Supplementary Figure 4Cii). The W_{50}, RT_{80}, and RT_{90} were all insignificant across the doses and paced frequencies, which align with other results found in literature (Mannhardt et al., 2016).

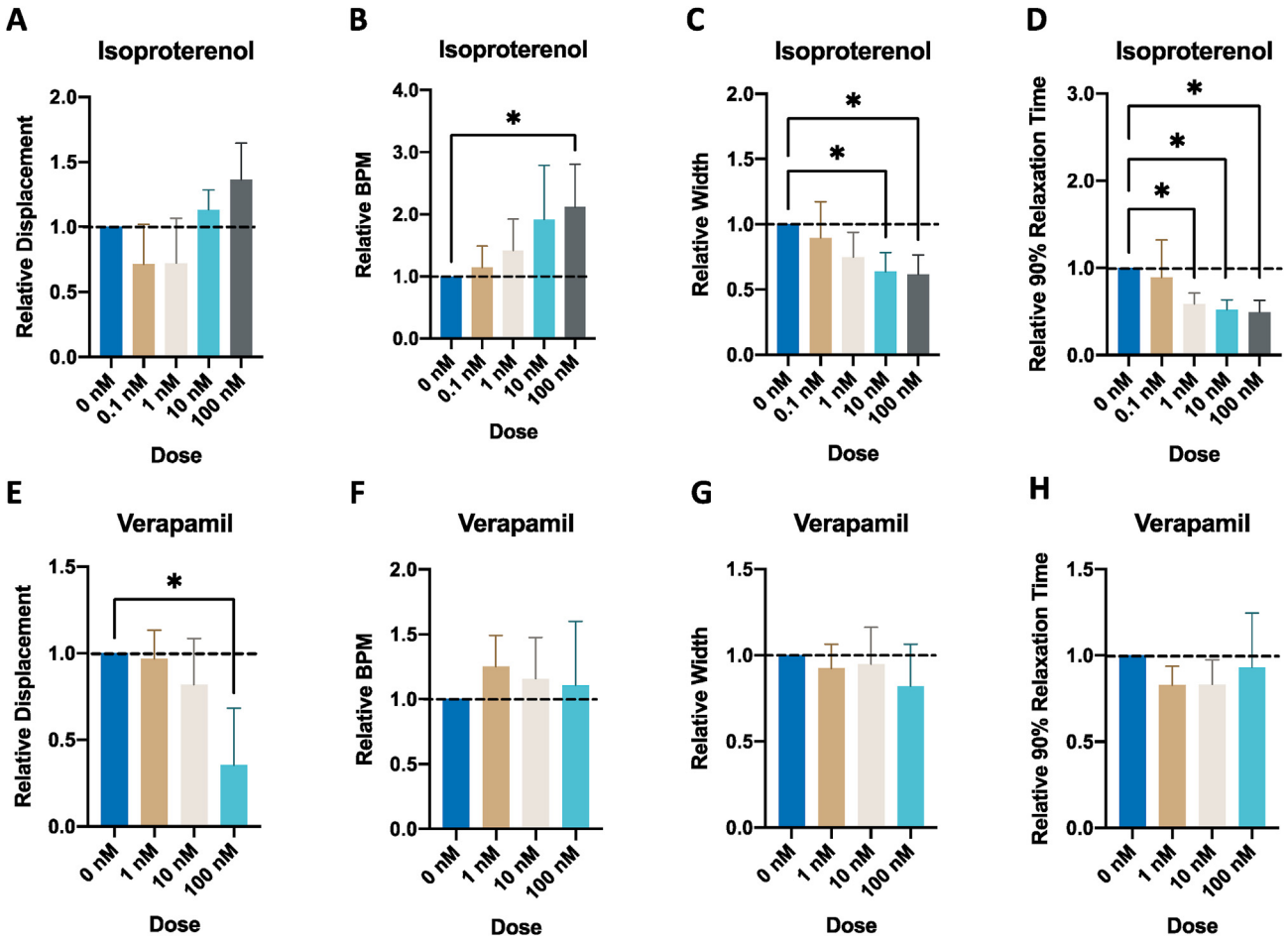

Fig. 4. Human cardiac micro-tissue drug response. Isoproterenol: Bar chart showing thin pillar displacement (A), BPM (B), width at half-height (C), and time at 90% peak relaxation (D) of unpaced cardiac micro-tissues over different doses (N = 3-4). (C) Example cardiac micro-tissue beating phenotype over different doses. Verapamil: Bar chart showing thin pillar displacement (E), BPM (F), width at half-height (G), and time at 90% peak relaxation (H) of unpaced cardiac micro-tissues over different doses (N = 4). Mean ± SD, *p ≤ 0.05, paired *t*-test.

4. Conclusion

This study demonstrated the ability of the μCOP system to fabricate a novel 3D hiPSC-CM based cardiac micro-tissue with physical alignment cues. The rapid printing speed made it possible to create many micro-tissues in a multiwell plate in a short time for high-throughput screening applications. The microscale printing resolution allowed us to print encapsulated hiPSC-CMs in 30 μm GelMA lines, leading to a high level of alignment after 7 days of culture through both alignment cues and stress cues from the two printed pillars. As a result, the cells exhibited a high level of maturity compared to their 2D plated cell control, displaying a significant increase in mRNA expression in at least 6 of the 8 maturity markers. As cell remodeling and proliferation from the fibroblasts were variable, we also successfully incorporated encapsulated fluorescent beads into the pillars. These beads allowed for robust tracking of small pillar movements for both data tracking and analysis, regardless of the tissue growth. Moreover, the entire model was printed onto a 5 mm coverslip, which can be easily fit into a 96-well plate for high-throughput drug testing. Since we recognized that both rapid, parallel image acquisition and analysis are also needed for a truly rapid drug testing model (Tiburcy et al., 2020), it is noteworthy that our technology of fabrication of micro-tissue is validated by the experiments using two drugs, ISO and VERA.

Notably, our results suggest we can still further improve hiPSC-CM maturity based on the findings that the expression levels of two of the tested maturity markers, SERCA2a and CXN43, were insignificant and inconclusive, respectively. As well, when comparing our drug responsivity metrics to literature, we found that Ronaldson-Bouchard et al. group produced a cardiac tissue with higher sensitivity to ISO (Ronaldson-Bouchard et al., 2018). This suggests that electrical training of our cardiac constructs, similar to this group, would be beneficial for improving maturity, and therefore drug sensitivity, and warrants the exploration of the study.

Since 3D micro-tissues are an important step to predict the drug efficacy and to confirm the safety before human trials, many researchers have designed and created 3D cardiac models. Our rapid 3D bioprinting technology provides the fast and accurate alignment of cardiac cells and other cells simultaneously while maintaining viability. The physical alignment cues from ECM have been shown to improve the functionality of cardiac tissues and are thus advantageous over similar pillar models relying on only stress cues (Liu et al., 2020). Moreover, the rapid turnaround from design to printed structure is also a desirable feature when expanding to specialized disease models, enabling quick and specific optimization. Additionally, the use of hiPSC-CMs opens the possibility for patient-specific disease testing. By taking cells from a patient and reprogramming them, a patient-derived cardiac tissue could help research more accurately target viable drugs before introduction into a human. Furthermore, the modular design innate to printing on a coverslip enables our model to be expanded into use in multi-organ-on-a-chip systems. We believe this cardiac micro-tissue can help to promote drug safety, efficacy, and personalized medicine.

Declaration of competing interest

The authors declare the following financial interests/personal relationships which may be considered as potential competing interests: SC is a co-founder of and has an equity interest in Allegro 3D, Inc., and he serves on the scientific advisory board. Some of his research grants, including those acknowledged here, have been identified for conflict of interest management based on the overall scope of the project and its potential benefit to Allegro 3D, Inc. The author is required to disclose this relationship in publications acknowledging the grant support, however the research subject and findings reported here did not involve the company in any way and have no relationship with the business activities or scientific interests of the company. The terms of this arrangement have been reviewed and approved by the University of California San Diego in accordance with its conflict of interest policies. The other authors have no competing interests to declare.

Acknowledgements

This project is supported by a grant from Takeda Pharmaceutical Company Limited as a Sanford Takeda Innovation Alliance project and in part by the US National Science Foundation (1903933). The authors also would like to acknowledge the University of California San Diego Neuroscience Microscopy Shared Facility funded by the National Institutes of Health (NS047101). The authors thank Dr. Tadahiro Shinozawa, Kohei Deguchi for their critical advice on our research work, and Dr. Yoji Ueda for project alliance management.

Appendix A. Supplementary data

Supplementary data to this article can be found online at https://doi.org/10.1016/j.ooc.2021.100007.

References

Agarwal, A., Goss, J.A., Cho, A., McCain, M.L., Parker, K.K., 2013. Microfluidic heart on a chip for higher throughput pharmacological studies. Lab Chip 13, 3599–3608. https://doi.org/10.1039/c3lc50350j.

Bertlein, S., Brown, G., Lim, K.S., Jungst, T., Boeck, T., Blunk, T., Tessmar, J., Hooper, G.J., Woodfield, T.B.F., Groll, J., 2017. Thiol–ene clickable gelatin: a platform bioink for multiple 3D biofabrication Technologies. Adv. Mater. 29, 1–6. https://doi.org/10.1002/adma.201703404.

Boudou, T., Legant, W.R., Mu, A., Borochin, M.A., Thavandiran, N., Radisic, M., Zandstra, P.W., Epstein, J.A., Margulies, K.B., Chen, C.S., 2012. A microfabricated platform to measure and manipulate the mechanics of engineered cardiac microtissues. Tissue Eng. Part A. 18, 910–919. https://doi.org/10.1089/ten.tea.2011.0341.

Duan, B., 2017. State-of-the-Art review of 3D bioprinting for cardiovascular tissue engineering. Ann. Biomed. Eng. 45, 195–209. https://doi.org/10.1007/s10439-016-1607-5.

Fairbanks, B.D., Schwartz, M.P., Bowman, C.N., Anseth, K.S., 2009. Photoinitiated polymerization of PEG-diacrylate with lithium phenyl-2,4,6-trimethylbenzoylphosphinate: polymerization rate and cytocompatibility. Biomaterials 30, 6702–6707. https://doi.org/10.1016/j.biomaterials.2009.08.055.

Gauvin, R., Chen, Y.C., Lee, J.W., Soman, P., Zorlutuna, P., Nichol, J.W., Bae, H., Chen, S., Khademhosseini, A., 2012. Microfabrication of complex porous tissue engineering scaffolds using 3D projection stereolithography. Biomaterials 33, 3824–3834. https://doi.org/10.1016/j.biomaterials.2012.01.048.

Guo, Y., Pu, W.T., 2020. Cardiomyocyte maturation: New phase in development. Circ. Res. 1086–1106. https://doi.org/10.1161/CIRCRESAHA.119.315862.

Hansen, A., Eder, A., Bönstrup, M., Flato, M., Mewe, M., Schaaf, S., Aksehirlioglu, B., Schwörer, A., Uebeler, J., Eschenhagen, T., 2010. Development of a drug screening platform based on engineered heart tissue. Circ. Res. 107, 35–44. https://doi.org/10.1161/CIRCRESAHA.109.211458.

Hinson, J.T., Chopra, A., Nafissi, N., Polacheck, W.J., Craig, C., Swist, S., Gorham, J., Yang, L., Schafer, S., Calvin, C., Haghighi, A., Homsy, J., Hubner, N., Church, G., Cook, A., Linke, W.A., Chen, C.S., Seidman, J.G., 2015. Titin mutations in iPS cells define sarcomere insufficiency as a cause of dilated cardiomyopathy john. Science 349 (80), 982–986. https://doi.org/10.1126/science.aaa5458.

Huebsch, N., Loskill, P., Deveshwar, N., Spencer, C.I., Judge, L.M., Mandegar, M.A., Fox, C.B., Mohamed, T.M.A., Ma, Z., Mathur, A., Sheehan, A.M., Truong, A., Saxton, M., Yoo, J., Srivastava, D., Desai, T.A., So, P.L., Healy, K.E., Conklin, B.R., 2016. Miniaturized iPS-cell-derived cardiac muscles for physiologically relevant drug response analyses. Sci. Rep. 6, 1–12. https://doi.org/10.1038/srep24726.

Kranias, E.G., Hajjar, R.J., 2012. Modulation of cardiac contractility by the phopholamban/SERCA2a regulatome. Circ. Res. 110, 1646–1660. https://doi.org/10.1161/CIRCRESAHA.111.259754.

Lim, K.S., Levato, R., Costa, P.F., Castilho, M.D., Alcala-Orozco, C.R., Van Dorenmalen, K.M.A., Melchels, F.P.W., Gawlitta, D., Hooper, G.J., Malda, J., Woodfield, T.B.F., 2018. Bio-resin for high resolution lithography-based biofabrication of complex cell-laden constructs. Biofabrication 10. https://doi.org/10.1088/1758-5090/aac00c.

Lin, H., Zhang, D., Alexander, P.G., Yang, G., Tan, J., Cheng, A.W.M., Tuan, R.S., 2013. Application of visible light-based projection stereolithography for live cell-scaffold fabrication with designed architecture. Biomaterials 34, 331–339. https://doi.org/10.1016/j.biomaterials.2012.09.048.

Lind, J.U., Yadid, M., Perkins, I., Connor, B.B.O., Eweje, F., Chantre, C.O., Hemphill, M.A., Yuan, H., Campbell, P.H., Vlassak, J.J., Parker, K.K., 2017. Cardiac microphysiological devices with flexible thin-film sensors for higher-throughput drug screening. Lab Chip 17, 3692–3703. https://doi.org/10.1039/c7lc00740j.

Liu, J., Miller, K., Ma, X., Dewan, S., Lawrence, N., Whang, G., Chung, P., McCulloch, A.D., Chen, S., 2020. Direct 3D bioprinting of cardiac micro-tissues mimicking native myocardium. Biomaterials 256, 1–10. https://doi.org/10.1016/j.biomaterials.2020.120204.

Ma, X., Qu, X., Zhu, W., Li, Y.Y.-S.Y., Yuan, S., Zhang, H., Liu, J., Wang, P., Lai, C.S.E., Zanella, F., Feng, G.-S., Sheikh, F., Chien, S., Chen, S., 2016. Deterministically patterned biomimetic human iPSC-derived hepatic model via rapid 3D bioprinting. Proc. Natl. Acad. Sci. 113, 1–6. https://doi.org/10.1073/pnas.1524510113.

Ma, X., Liu, J., Zhu, W., Tang, M., Lawrence, N., Yu, C., Gou, M., Chen, S., 2018. 3D bioprinting of functional tissue models for personalized drug screening and in vitro disease modeling. Adv. Drug Deliv. Rev. 132, 235–251. https://doi.org/10.1016/j.addr.2018.06.011.

Ma, X., Dewan, S., Liu, J., Tang, M., Miller, K.L., Yu, C., Lawrence, N., McCulloch, A.D., Chen, S., 2019. 3D printed micro-scale force gauge arrays to improve human cardiac tissue maturation and enable high throughput drug testing. Acta Biomater. 95, 319–327. https://doi.org/10.1016/j.actbio.2018.12.026.

Mannhardt, I., Breckwoldt, K., Letuffe-Brenière, D., Schaaf, S., Schulz, H., Neuber, C., Benzin, A., Werner, T., Eder, A., Schulze, T., Klampe, B., Christ, T., Hirt, M.N., Huebner, N., Moretti, A., Eschenhagen, T., Hansen, A., 2016. Human engineered heart tissue: analysis of contractile force. Stem Cell Reports 7, 29–42. https://doi.org/10.1016/j.stemcr.2016.04.011.

Mathur, A., Loskill, P., Shao, K., Huebsch, N., Hong, S.G., Marcus, S.G., Marks, N., Mandegar, M., Conklin, B.R., Lee, L.P., Healy, K.E., 2015. Human iPSC-based cardiac microphysiological system for drug screening applications. Sci. Rep. 5, 1–7. https://doi.org/10.1038/srep08883.

Mathur, A., Ma, Z., Loskill, P., Jeeawoody, S., Healy, K.E., 2016. In vitro cardiac tissue models: current status and future prospects. Adv. Drug Deliv. Rev. 96, 203–213. https://doi.org/10.1016/j.addr.2015.09.011.

Munoz, Z., Shih, H., Lin, C.-C., 2014. Gelatin hydrogels formed by orthogonal thiol-norbornene photochemistry for cell encapsulation. Biomater. Sci. 2, 1063–1072. https://doi.org/10.1039/c4bm00070f.

Nichol, J.W., Koshy, S.T., Bae, H., Hwang, C.M., Yamanlar, S., Khademhosseini, A., 2010. Cell-laden microengineered gelatin methacrylate hydrogels. Biomaterials 31, 5536–5544. https://doi.org/10.1016/j.biomaterials.2010.03.064.

Nunes, S.S., Miklas, J.W., Liu, J., Aschar-Sobbi, R., Xiao, Y., Zhang, B., Jiang, J., Massé, S., Gagliardi, M., Hsieh, A., Thavandiran, N., Laflamme, M.A., Nanthakumar, K., Gross, G.J., Backx, P.H., Keller, G., Radisic, M., 2013. Biowire: a platform for maturation of human pluripotent stem cell–derived cardiomyocytes. Nat. Methods 10, 781–787. https://doi.org/10.1038/nmeth.2524.

Okai, Y., Matsune, K., Yamanaka, K., Matsui, T., Pfeiffer Kaushik, E., Harada, K., Kohara, H., Miyawaki, A., Ozaki, H., Wagoner, M., Shinozawa, T., 2020. Video-based assessment of drug-induced effects on contractile motion properties using human induced pluripotent stem cell-derived cardiomyocytes. J. Pharmacol. Toxicol. Methods 105. https://doi.org/10.1016/j.vascn.2020.106893.

Rao, C., Prodromakis, T., Kolker, L., Chaudhry, U.A.R., Trantidou, T., Sridhar, A., Weekes, C., Camelliti, P., Harding, S.E., Darzi, A., Yacoub, M.H., Athanasiou, T., Terracciano, C.M., 2013. The effect of microgrooved culture substrates on calcium cycling of cardiac myocytes derived from human induced pluripotent stem cells. Biomaterials 34, 2399–2411. https://doi.org/10.1016/j.biomaterials.2012.11.055.

Ronaldson-Bouchard, K., Ma, S.P., Yeager, K., Chen, T., Song, L.J., Sirabella, D., Morikawa, K., Teles, D., Yazawa, M., Vunjak-Novakovic, G., 2018. Advanced maturation of human cardiac tissue grown from pluripotent stem cells. Nature 556, 239–243. https://doi.org/10.1038/s41586-018-0016-3.

Ruskowitz, E.R., Deforest, C.A., 2019. Proteome-wide analysis of cellular response to ultraviolet light for biomaterial Synthesis and modification. ACS Biomater. Sci. Eng. 5, 2111–2116. https://doi.org/10.1021/acsbiomaterials.9b00177.

Salick, M.R., Napiwocki, B.N., Sha, J., Knight, G.T., Chindhy, S.A., Kamp, T.J., Ashton, R.S., Crone, W.C., 2014. Micropattern width dependent sarcomere development in human ESC-derived cardiomyocytes. Biomaterials 35, 4454–4464. https://doi.org/10.1016/j.biomaterials.2014.02.001.

Sanguinetti, M., Tristani-Firouzi, M., 2006. hERG potassium channels and cardiac arrhythmia. Nature 440, 463–469. https://doi.org/10.1038/nature04710.

Seguchi, O., Takashima, S., Yamazaki, S., Asakura, M., Asano, Y., Shintani, Y., Wakeno, M., Minamino, T., Kondo, H., Furukawa, H., Nakamaru, K., Naito, A., Takahashi, T., Ohtsuka, T., Kawakami, K., Isomura, T., Kitamura, S., Tomoike, H., Mochizuki, N., Kitakaze, M., 2007. A cardiac myosin light chain kinase regulates sarcomere assembly in the vertebrate heart. J. Clin. Invest. 117, 2812–2824. https://doi.org/10.1172/JCI30804.

Sottas, V., Wahl, C.M., Trache, M.C., Bartolf-Kopp, M., Cambridge, S., Hecker, M., Ullrich, N.D., 2018. Improving electrical properties of iPSC-cardiomyocytes by

enhancing Cx43 expression. J. Mol. Cell. Cardiol. 120, 31–41. https://doi.org/10.1016/j.yjmcc.2018.05.010.

Stoehr, A., Neuber, C., Baldauf, C., Vollert, I., Friedrich, F.W., Flenner, F., Carrier, L., Eder, A., Schaaf, S., Hirt, M.N., Aksehirlioglu, B., Tong, C.W., Moretti, A., Eschenhagen, T., Hansen, A., 2014. Automated analysis of contractile force and Ca2+ transients in engineered heart tissue. Am. J. Physiol. Heart Circ. Physiol. 306, 1353–1363. https://doi.org/10.1152/ajpheart.00705.2013.

Suri, S., Han, L.-H., Zhang, W., Singh, A., Chen, S., Schmidt, C.E., 2011. Solid freeform fabrication of designer scaffolds of hyaluronic acid for nerve tissue engineering. Biomed. Microdevices 13, 983–993. https://doi.org/10.1007/s10544-011-9568-9.

Takeda, M., Miyagawa, S., Fukushima, S., Saito, A., Ito, E., Harada, A., Matsuura, R., Iseoka, H., Sougawa, N., Mochizuki-Oda, N., Matsusaki, M., Akashi, M., Sawa, Y., 2018. Development of in vitro drug-induced cardiotoxicity assay by using three-dimensional cardiac tissues derived from human induced pluripotent stem cells. Tissue Eng. C Methods 24, 56–67. https://doi.org/10.1089/ten.tec.2017.0247.

Tiburcy, M., Meyer, T., Liaw, N.Y., Zimmermann, W.-H., 2020. Generation of engineered human myocardium in a multi-well format. STAR Protoc 1. https://doi.org/10.1016/j.xpro.2020.100032, 100032.

Turnbull, I.C., Karakikes, I., Serrao, G.W., Backeris, P., Lee, J.J., Xie, C., Senyei, G., Gordon, R.E., Li, R.A., Akar, F.G., Hajjar, R.J., Hulot, J.S., Costa, K.D., 2014. Advancing functional engineered cardiac tissues toward a preclinical model of human myocardium. FASEB J 28, 644–654. https://doi.org/10.1096/fj.13-228007.

Veldhuizen, J., Migrino, R.Q., Nikkhah, M., 2019. Three-dimensional microengineered models of human cardiac diseases. J. Biol. Eng. 13, 1–12. https://doi.org/10.1186/s13036-019-0155-6.

Yu, C., Miller, K.L., Schimelman, J., Wang, P., Zhu, W., Ma, X., Tang, M., You, S., Lakshmipathy, D., He, F., Chen, S., 2020. A sequential 3D bioprinting and orthogonal bioconjugation approach for precision tissue engineering. Biomaterials 258, 1–12. https://doi.org/10.1016/j.biomaterials.2020.120294.

Zuppinger, C., 2019. 3D cardiac cell culture: a critical review of current Technologies and applications. Front. Cardiovasc. Med. 1–9. https://doi.org/10.3389/fcvm.2019.00087.